Copyright WILEY-VCH Verlag GmbH & Co. KGaA, 69469 Weinheim, Germany, 2015.

ADVANCED MATERIALS

Supporting Information

for *Adv. Mater.,* DOI: 10.1002/adma.201500039

# An Optoelectronic Resistive Switching Memory with Integrated Demodulating and Arithmetic Functions

*Hongwei Tan, Gang Liu,* Xiaojian Zhu, Huali Yang, Bin Chen, Xinxin Chen, Jie Shang, Wei D. Lu, Yihong Wu, and Run-Wei Li**

# Supporting Information

Copyright WILEY-VCH Verlag GmbH & Co. KGaA, 69469 Weinheim, Germany, 20

**An Optoelectronic Resistive Switching Memory with Integrated Demodulating and Arithmetic Functions**

*Hongwei Tan, Prof. Dr. Gang Liu,* Dr. Xiaojian Zhu, Huali Yang, Dr. Bin Chen, Xinxin Chen, Dr. Jie Shang, Prof. Dr. Yihong Wu, and Prof. Dr. Run-Wei Li**

H. W. Tan, Prof. Dr. G. Liu, Dr. X. J. Zhu, H. L. Yang, Dr. B. Chen, X. X. Chen, Dr. J. Shang, Prof. Dr. R.-W. Li
Key Laboratory of Magnetic Materials and Devices,
Ningbo Institute of Materials Technology and Engineering, Chinese Academy of Sciences
Ningbo, 315201, P. R. China
Zhejiang Province Key Laboratory of Magnetic Materials and Application Technology,
Ningbo Institute of Materials Technology and Engineering, Chinese Academy of Sciences
Ningbo, 315201, P. R. China
E-mail: runweili@nimte.ac.cn; liug@nimte.ac.cn
Prof. Dr. Y. H. Wu
Information Storage Materials Laboratory,
Department of Electrical and Computer Engineering,
National University of Singapore, 4 Engineering Drive 3
Singapore 117583

**Keywords:** Adjustable photoconductivity, resistive switching, non-volatile memory, information demodulating, arithmetic

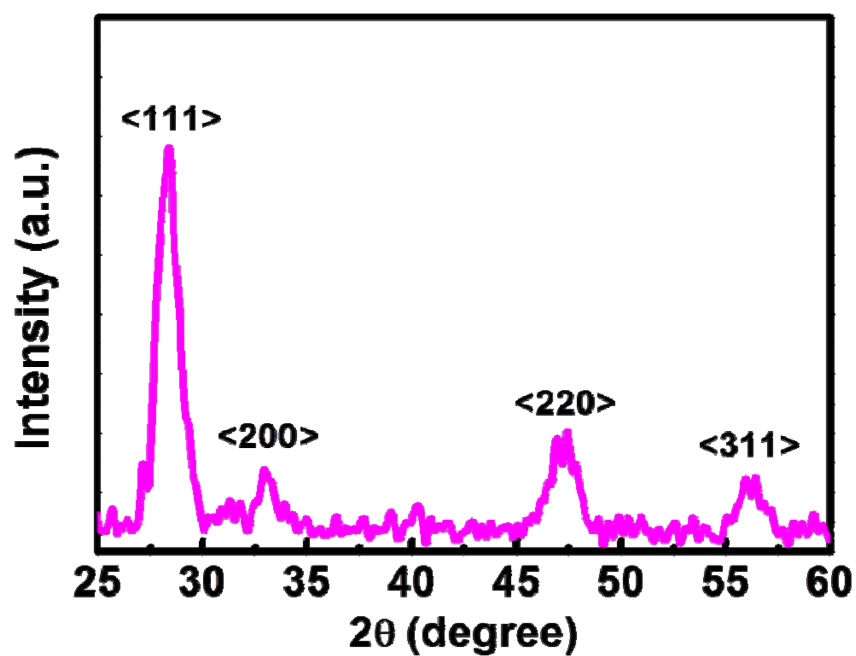


**Figure S1.** Glazing-incidence X-ray diffractive (GIXRD) pattern of the $CeO_{2-x}$ layer deposited on $AlO_y/Al/SiO_2/Si$ multilayers.

The as-sputtered $CeO_{2-x}$ film exhibits XRD peaks at 28.4°, 32.9°, 47.2° and 56.2°, respectively, which correspond to the <111>, <200>, <220> and <311> planes of the polycrystalline fluorite structured cerium oxide.

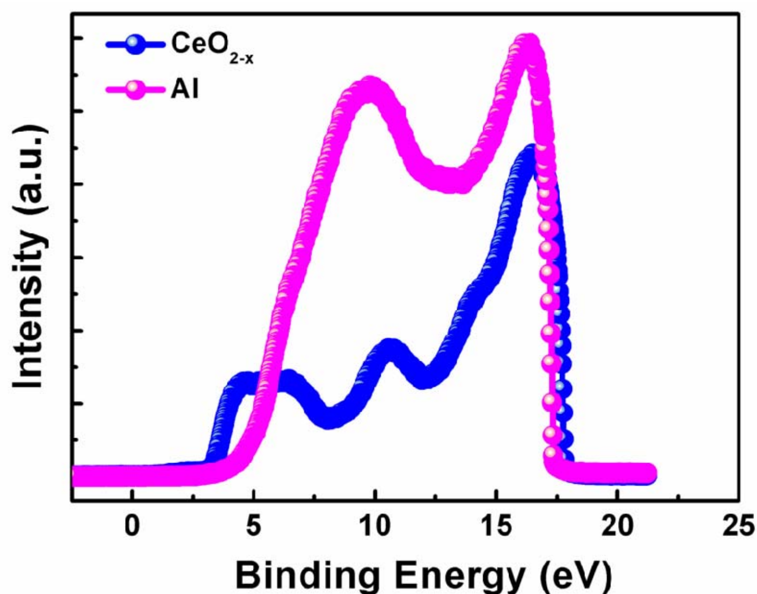


**Figure S2.** Ultraviolet photoelectron spectra (UPS) of the $CeO_{2-x}$ thin film and the Al electrode.

The work function $\chi$ can be calculated from the bonding energy cut-off at the high-energy end of the UPS spectrum according to the following equation:

$$\chi = h\nu - E_{cutoff} \tag{1}$$

where $h\nu$ is the photon energy of the ultraviolet radiation source and is 21.2 eV in the present study, and $E_{cutoff}$ is the cut-off binding energy of secondary electrons which can be estimated with the following equation:

$$E_{cutoff} = \frac{E_{Bh} + E_{Bl}}{2} \tag{2}$$

where $E_{Bh}$ and $E_{Bl}$ are the binding energies read in the spectrum where the corresponding intensities are 80% and 20% of the UPS signal maximum at the high-energy end, respectively. Using the above equations, the work functions of the $CeO_{2-x}$ thin film and Al electrode are estimated to be 3.65 eV and 4.13 eV, respectively. As such, a Schottky junction is established at the $CeO_{2-x}/AlO_y/Al$ interfacial region.

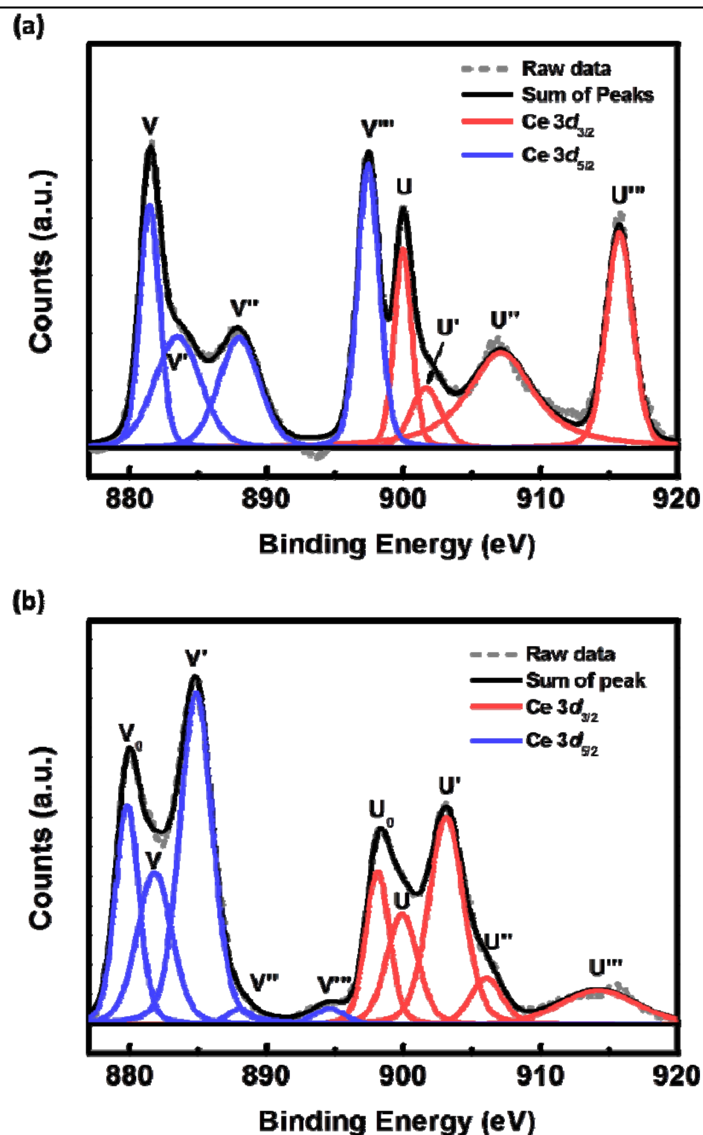


**Figure S3.** Core-level Ce 3*d* X-ray photoelectron spectra (XPS) recorded (**a**) on the surface of and (**b**) inside the $CeO_{2-x}$ thin film deposited on $AlO_y$/Al-coated substrate.

The X-ray photoelectron spectroscopic (XPS) measurements were carried out to investigate the surface and internal chemical compositions of, as well as to confirm the presence of oxygen vacancies in the $CeO_{2-x}$ thin films that have been deposited on the $AlO_y$/Al-coated substrates, using an ion-etching treatment for the depth-profiling of the cerium oxide films. The oxidation state of the cerium species was examined with the cerium 3*d* spectra as shown in **Figure S3(a)**, where the binding energies were calibrated using the C 1s peak as a reference. The XPS spectra of the Ce 3*d* level can be curve-fitted into eight characteristic peaks. The peaks with the binding energies (BEs) of 881.4 eV (V), 883.5 eV (V’), 888.0 eV

(V'') and 897.4 eV (V''') can be attributed to the Ce $3d_{5/2}$ components, while the peaks with the BEs of 899.9 eV (U), 901.6 eV (U'), 907.1 eV (U'') and 915.8 eV (U''') are ascribed to the Ce $3d_{3/2}$ components.[1,2] The peak with the BE of 883.5 eV (V') corresponds to the $3d^{10}4f^{1}$ electronic state of the trivalent $Ce^{3+}$ ion, while the peaks with the BEs of 897.4 eV (V''') and 915.8 eV (U''') represent the $3d^{10}4f^{0}$ electronic state corresponding to the tetravalent $Ce^{4+}$ ion. The copresence of $Ce^{3+}$ and $Ce^{4+}$ reveals that oxygen vacancies exist on the surface of the as prepared $CeO_{2-x}$ films.

On the other hand, the XPS core-level Ce 3*d* spectra of the $CeO_{2-x}$ film recorded at the depth of ~ 20 nm, which is in close proximity to the $AlO_y$/Al interface, shows a significant change in the line shape (**Figure S3(b)**). For instance, the trivalent $Ce^{3+}$ ion with the BE of 883.5 eV (V') shows an obvious increase in the intensity, while the tetravalent $Ce^{4+}$ ion species with the BEs of 897.4 eV (V''') and 915.8 eV (U''') decrease accordingly. In addition, the newly appeared peaks with the BEs of 879.8 eV ($V_0$) and 898.1 eV ($U_0$) in **Figure S3(b)** also correspond to the increasing amount of trivalent $Ce^{3+}$ ions. Therefore, it proves that the concentration of the $Ce^{3+}$ species, or the oxygen vacancies, increases when sampling from the ITO/$CeO_{2-x}$ towards the $CeO_{2-x}$/$AlO_y$ interfaces. This is in good agreement with the asymmetric structure of the ITO/$CeO_{2-x}$/$AlO_y$/Al devices, wherein the surface layer of $CeO_{2-x}$ will get more oxidized when the sample is transferred in air from the magnetron sputter to the PLD system, while the $AlO_y$/Al layer will act as a reservior to grab oxygen content during the $CeO_{2-x}$ deposition process and generate more oxygen vacancies in the cerium oxide film near the $CeO_{2-x}$/$AlO_y$/Al interface.

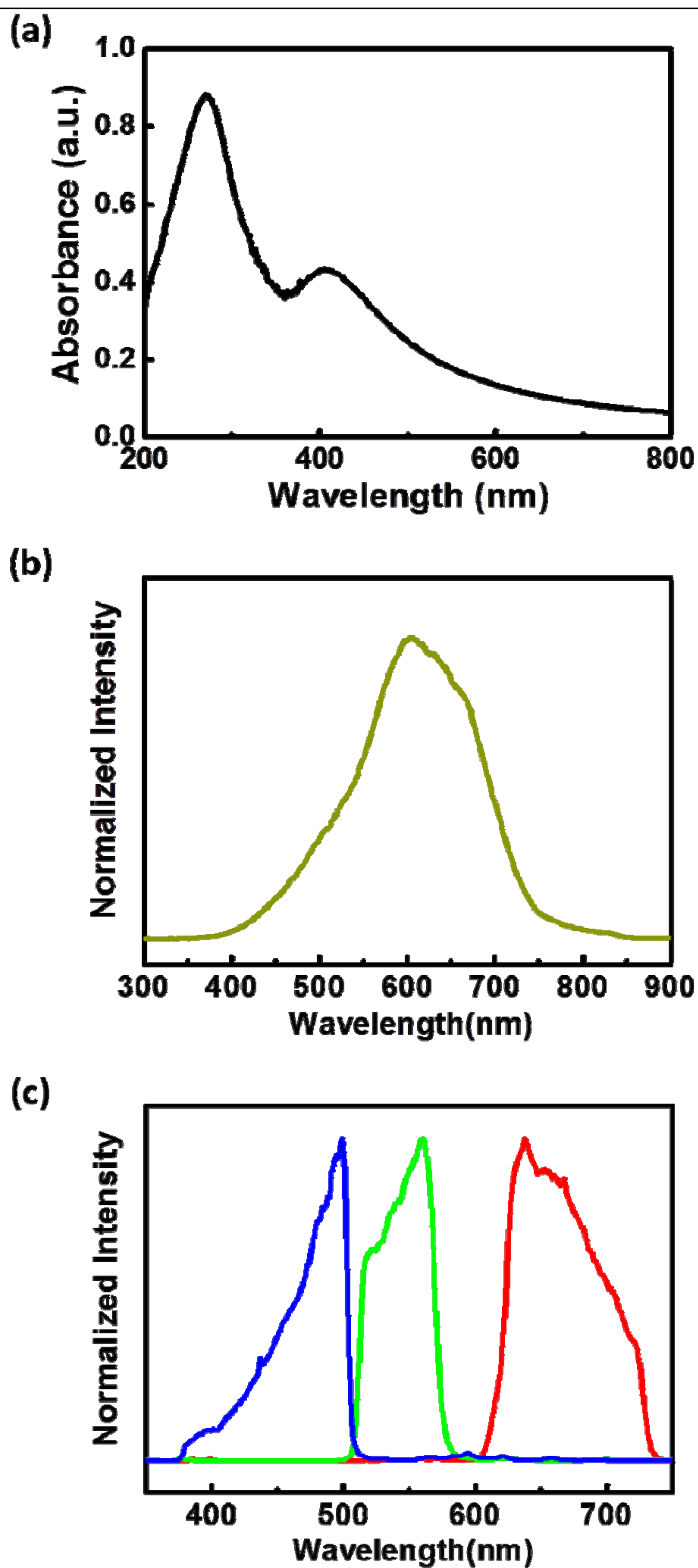


**Figure S4.** (**a**) UV-Visible absorption spectrum of the $CeO_{2-x}$ thin film. (**b**) Broadband and (**c**) red, blue and green emission spectra of the halogen lamp.

The as-prepared $CeO_{2-x}$ thin film shows an absorption peak centered at the wavelength of ~ 300 nm as well as a moderate absorption band over the entire 400 nm - 800 nm visible region (**Figure S4(a)**). The halogen lamp of the probe station, which is normally used for illumination and sample visualization with a broadband emission spectra over the 400 nm - 800 nm and a peak maximum at 606 nm (**Figure S4(b)**), has been used as the optical illumination/information source in the present study. The visible light can be further filtered into red, green and blue light beams with the maximum emission at 638 nm, 560 nm and 499 nm, respectively, which are the primary colors of light that can be mixed with different proportions to generate a wide range of additive colors (**Figure S4(c)**).

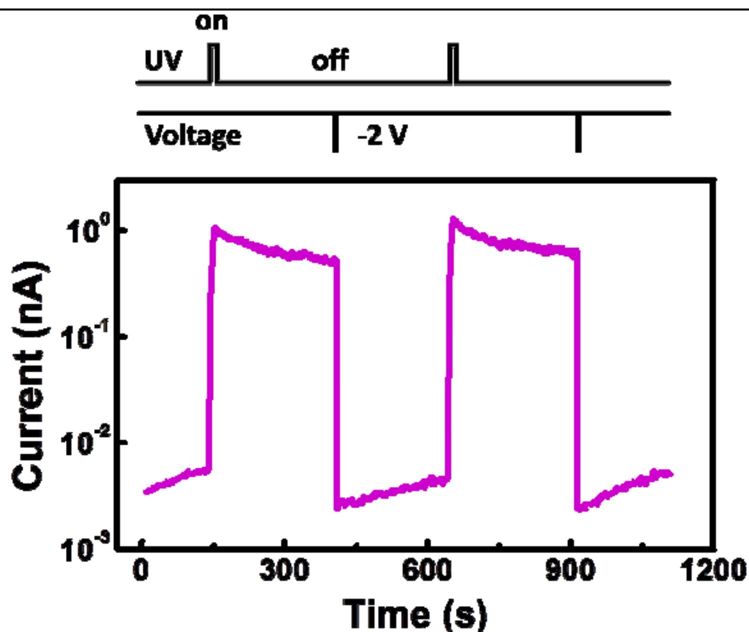


**Figure S5.** Persistent and electrically erasable photoconductivity of the ITO/$CeO_{2-x}$/$AlO_y$/Al structured devices in response to the 254 nm UV light. The optical illumination intensity and duration are 3 fW/μm$^2$ and 10 s, respectively. The read voltage is 0.1 V and the erase voltage is -2 V with 0.1 s.

UV light with the wavelength of 254 nm, intensity of 3 fW/μm$^2$ and illumination duration of 10 s can program the device to a lower state with the resistance of ~ $10^8$ Ω at the read voltage of 0.1 V. The photoresponse to UV light is persistent, and can be erased with a voltage with the height of -2 V and duration of 0.1 s.

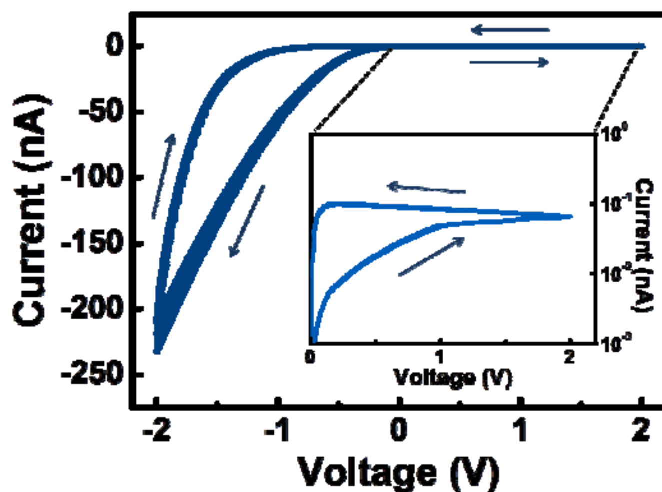


**Figure S6.** Electrically resistive switching behavior of the ITO/$CeO_{2-x}$/$AlO_y$/Al structured devices.

When the device is measured in the dual-sweep mode, electrically resistive switching behaviors with the ON/OFF ratio of 10 read at 0.1 V is also observed. The electrically resistive switching may be ascribed to the electric field-induced migration of oxygen vacancies.[3]

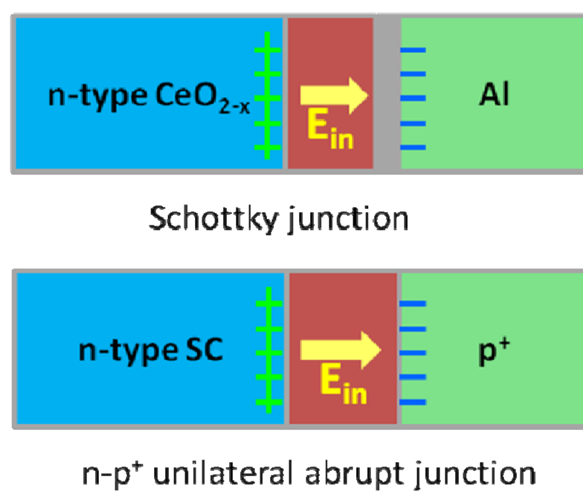


**Figure S7.** Schematic illustration of the $CeO_{2-x}/AlO_y/Al$ (upper panel) junction and an n-$p^+$ unilateral abrupt junction.

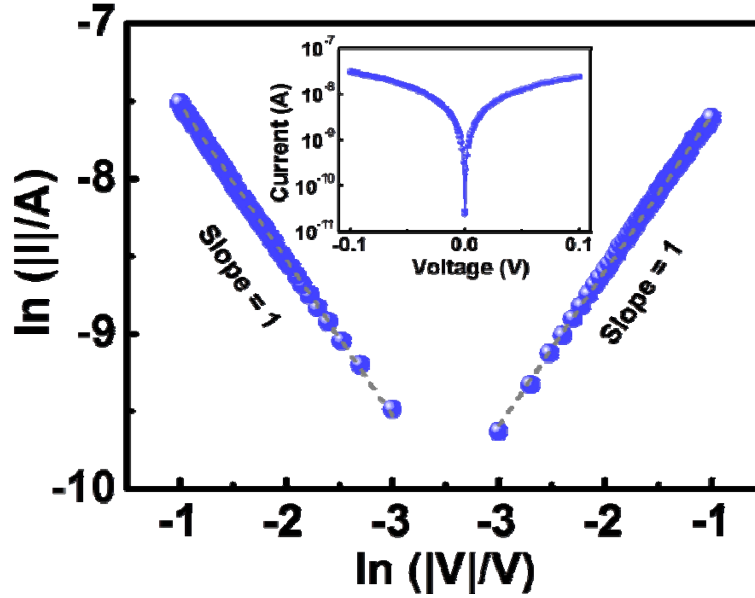


**Figure S8.** Experimental and fitted current-voltage (*I*-*V*) characteristics of the ITO/$CeO_{2-x}$/$AlO_y$/Al multilayer structured device monitored upon being exposed to broadband illumination with the intensity of 59.6 pW/μm$^2$ and the duration of 100 s in log-log scale. Inset shows the same experimental data plotted in linear-log scale.

Since cerium oxide has been widely accepted as n-type semiconductors while the 5 nm $AlO_y$ layer serves as a tunneling barrier to suppress the dark current,[4-6] the $CeO_{2-x}$/$AlO_y$/Al junction well resembles the structure of an n-p$^+$ unilateral abrupt junction (**Figure S7**).[7] The width ($W_D$) of the depletion region (or the interfacial space-charge layer in $CeO_{2-x}$ film next to the $AlO_y$ layer) can be estimated with the following equation:[7]

$$W_D = \sqrt{\frac{2\varepsilon_s \psi_{bi}}{qN}} \tag{3}$$

where $\varepsilon_s$ is the dielectric constant of $CeO_{2-x}$ layer, $\Psi_{bi}$ is the build-in potential of the depletion region, $q$ is the unit charge and $N$ is the concentration of the positively charged defects. Initially, $N$ equals to $N_0$ which is a constant determined by the intrinsic Fermi levels of the cerium oxide and the Al electrode. Upon being exposed to optical illumination, the trapped electrons will be excited and leaving photo-charged oxygen vacancies, the concentration of which shows a linear dependence on the illumination time $t$, so the total concentration of positively charged defects is described by the following equation instead:

$$N = N_0 + \Delta N = N_0 + at \quad (4)$$

where $\Delta N$ is the concentration of positively photo-charged defects, $t$ is the illumination time, $a$ means the formation rate of photo-charged oxygen vacancies and is a constant under a certain optical conditions.

The position-dependent potential in the depletion region can be expressed as: [7]

$$\psi_{bi}(x) = |\varepsilon_m|(x - \frac{x^2}{2W_D}) \quad (5)$$

where $|\varepsilon_m|$ is the maximum electric field and $x$ is the position measured from the $CeO_{2-x}/AlO_y$ interface. Therefore, the build-in potential of the depletion region can be described as :

$$\psi_{bi} = \psi_{bi}(W_D) - \psi_{bi}(0) = \frac{1}{2}|\varepsilon_m|W_D \quad (6)$$

Thus, with equations (3) and (6), the width of depletion can be derives as:

$$W_D = \frac{\varepsilon_s|\varepsilon_m|}{q(N_D + at)} \quad (7)$$

In addition, **Figure S8** suggests that the conduction behavior of the ITO/$CeO_{2-x}/AlO_y$/Al multilayer structured device under optical illumination is ohmic in nature, where the Ohm's law applies:

$$J = \sigma E \quad (8)$$

where $J$ is the current density flowing through the device, σ is the conductivity of depletion region and $E$ is the strength of the electric field. Generally, the voltage applied across the ITO/$CeO_{2-x}/AlO_y$/Al structure will almost drop at the depletion region,[5] thus the electric field can be expresses as:

$$E = \frac{V}{W_D} \quad (9)$$

where $V$ is the voltage applied onto the device and is the read voltage in the present study. Finally, the current density can be expressed as

$$J = \frac{\sigma V q a}{\varepsilon_s |\varepsilon_m|}(t + \frac{N_D}{a}) = A(t + b) \quad (10)$$

and shows a linear dependence on the illumination time $t$, where $A = \frac{\sigma V q a}{\varepsilon_s |\varepsilon_m|}$ and $b = \frac{N_D}{a}$. This linear relationship is in good agreement with the experimental results of **Figure 2(c)**, which plots the photoresponse of the ITO/$CeO_{2-x}$/$AlO_y$/Al multilayer structured device as a function of time under different broadband optical illumination intensities. Therefore, the proposed photoresponse mechanism, wherein the photo-charged oxygen vacancies at the interficial region significantly modulate the band bending at the $CeO_{2-x}$/$AlO_y$/Al region, can be confidently verified. Similarly, the device current also shows a linear dependence on the total optical pulse number $n$, according to the following equation

$$J = \frac{\sigma V q a'}{\varepsilon_s |\varepsilon_m|}(n + \frac{N_D}{a'}) = A'(n + b') \quad (11)$$

where $A' = \frac{\sigma V q a'}{\varepsilon_s |\varepsilon_m|}$, $b' = \frac{N_D}{a'}$, $a'$ is the amount of photo-charged oxygen vacancies generated per optical pulse and is a constant under a certain optical conditions.

**References**

[1] D. Chu, Y. Masuda, T. Ohji, K. Kato, *Phys. Status. Solidi. A* **2012**, *209*, 139.

[2] A. Younis, D. Chu, S. Li, *J. Phys. D: Appl. Phys.* **2012**, *45*, 355101.

[3] J. Shang, G. Liu, H. Yang, X. Zhu, X. Chen, H. Tan, B. Hu, L. Pan, W. Xue, R.-W. Li, *Adv. Funct. Mater.* **2014**, *24*, 2171.

[4] X. Qi, Y. S. Lin, C. T. Holt, S. L. Swartz, *J. Mater. Sci.* **2003**, *38*, 1073.

[5] P. Jasinski, T. Suzuki, H. U. Anderson, *Sens. Actuators B* **2003**, *95*, 73.

[6] D. W. Lee, J. W. Lee, T. S. Jang, B. K. Kim, *J. Ceram. Process. Res.* **2006**, *7*, 148.

[7] S. M. Sze, K. K. Ng, *Physics of Semiconductor Devices*, 3rd Ed., Wiley-Interscience, Hoboken, NJ, USA **2007**, p. 136